Bistatic scattering from a canonical building

G. Di Martino, A. Di Simone, A. Iodice, D. Riccio, G. Ruello
Department of Information Technology and Electrical Engineering
University of Napoli Federico II
Napoli, Italy
alessio.disimone@unina.it

W. Fuscaldo
Department of Information Engineering, Electronics and Telecommunications
Sapienza University of Rome
Rome, Italy
walter.fuscaldo@uniroma1.it

***Abstract*—In this paper we present an analytical model for the evaluation of the electromagnetic (EM) scattering from a typical composite target of urban areas in a generic bistatic configuration. The considered scene comprises a canonical building modeled as a parallelepiped lying over a rough terrain. Closed-form expressions for the scattered EM field are derived under the framework of the Kirchhoff approximation, with subsequent Geometrical Optics and Physical Optics approximations adopted for evaluating scattering from building walls and ground, respectively. Single- and multiple-scattering contributions are properly modeled as well as the EM and geometric characteristics of both the composite target and the sensors, such as material composition, size, terrain roughness, building orientation, viewing angle, polarization, frequency. The proposed scattering model can be used in information retrieval procedures using bistatic radar data.**

***Index Terms*—Electromagnetic scattering, Kirchhoff approximation, physical optics, radar cross section, bistatic radars.**

I. Introduction

Microwave remote sensing technologies represent a fundamental tool for urban areas monitoring and management [1]. However, a proper exploitation of remotely sensed data and the retrieval of accurate information require a challenging effort to be encompassed. Without a comprehensive understanding and quantitative modeling of the complex phenomenology behind data formation in urban areas, only basic information (shape, classification) related to the man-made structures can be inferred from single SAR images. Indeed, the development of analytical, reliable, and efficient models describing the interaction between electromagnetic (EM) waves and the illuminated objects paves the way for the design of accurate inversion procedures [2] and for an accurate interpretation of urban remote sensing data [3].

As opposed to natural surfaces which have been the subject of extensive studies within the EM scattering theory (see classical books on scattering theory from rough surfaces, e.g., [4], [5]), few efforts have been done by the scientific community in order to develop closed-form scattering models suited to urban areas. So far, the reference work is still that in [6] where EM scattering from a canonical building is studied in order to investigate the EM behavior of typical urban structures. There, a canonical urban scene consisting of an isolated building placed over rough terrain was considered and the related scattering problem was analyzed under the framework of Kirchhoff Approximation (KA) and the subsequent Geometrical Optics (GO) and Physical Optics (PO) solutions.

It is worth noting here that only backscattering was considered in [6] and, therefore, the models presented therein can be applied only to monostatic remote sensing systems, such as synthetic aperture radar (SAR). However, in the recent past, bi- and multi-static radar systems, such as bistatic SAR and passive bistatic radars have been experiencing a growing interest in the remote sensing community. Accordingly, in order to fully exploit the potentialities of such systems with respect to monostatic ones, the development of closed-form bistatic scattering models is advisable. In this direction, extensions to a more generic bistatic configuration of the model proposed in [6] have been recently presented in [7] and [8] for isotropic and anisotropic ground, respectively. Notwithstanding, both bistatic scattering models were derived under GO only.

Taking cues from these previous works, in this paper we propose the bistatic extension of the model in [6] but under zero-order PO and provide analytical expressions required to evaluate the bistatic radar cross section (RCS) of a canonical building.

The remainder of this work is as follows: Section II introduces the scattering problem and describes the proposed analytical model; some numerical results showing the impact of the building orientation on its overall RCS are presented and discussed in Section III. Concluding remarks are sketched in Section IV.

II. Theoretical Framework

The geometry of the scattering problem considered here is depicted in Fig. 1. The composite target consists of an isolated building modeled as a rectangular parallelepiped with smooth dielectric faces and placed on a rough terrain.

The reference system is built as in [6] and [7]: the $z = 0$ plane contains the mean plane of the ground surface; the x-axis is chosen so that the transmitting antenna lies in the

This work has been funded by the Department of Information Technology and Electrical Engineering, University of Napoli Federico II, Napoli, Italy, in the framework of the MORES project.

978-1-7281-8942-0/20/$31.00 ©2020 IEEE

Authorized licensed use limited to: Universita degli Studi di Napoli Federico II. Downloaded on January 05,2021 at 14:20:17 UTC from IEEE Xplore. Restrictions apply.

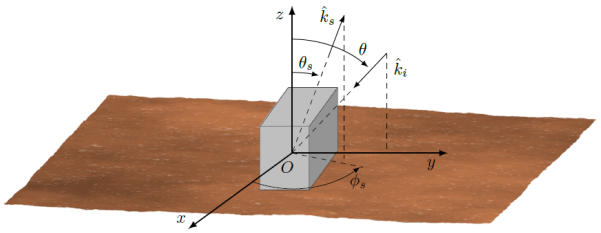

Fig. 1. Geometry and reference system for the considered composite target. A rectangular parallelepiped with smooth dielectric faces lying over a rough ground surface.

$x = 0$ plane. Both the transmitter and the receiver are assumed in the far-field region, which is a reasonable assumption in remote sensing applications. Accordingly, the position of the former is identified by the illumination angle θ only, whereas the position of the latter by the scattering look angle θ_s and azimuth angle ϕ_s.

Building walls have an arbitrary orientation with respect to the ground incidence plane. The smallest angle measured clockwise from the positive x semi-axis to the long wall base is the orientation angle $\phi \in [0, \pi]$ of the building. The unit vector normal to the m-th wall base is written as [7]

$$\hat{n}_{\mathrm{W}_m} = \sin\phi_m \hat{x} + \cos\phi_m \hat{y}, \quad m = 0, 1, 2, 3\,, \tag{1}$$

where $\phi_m = \phi + m\pi/2$.

The roughness of the underlying ground is modeled via a normally-distributed 2-dimensional stochastic process with zero mean and variance σ^2. Here, we limit our analysis to isotropic terrain surface with exponential normalized correlation function $\rho(\tau) = \exp(-\tau^2/l_\mathrm{c}^2)$, l_c standing for the surface correlation length. However, an extension of the proposed scattering model to anisotropic surfaces will be presented in [9].

According to [6] and [7], the incident electric field $\underline{E}_\mathrm{i}(\underline{r})$ is modeled as a plane wave with complex amplitude E_0, polarization state $\hat{e}_\mathrm{i}$ and propagation direction $\hat{k}_\mathrm{i}$. Therefore,

$$\underline{E}_\mathrm{i}(\underline{r}) = E_0 \hat{e}_\mathrm{i} \exp(jk\hat{k}_\mathrm{i} \cdot \underline{r}) \tag{2}$$

where $\underline{r}$ is the observation point, k is the EM wavenumber, $\hat{k}_\mathrm{i} = -\sin\theta\hat{y} - \cos\theta\hat{z}$.

Accordingly, under both KA-GO and KA-PO, the EM field $\underline{E}_\mathrm{s}(\underline{r})$ scattered from a surface A_0 separating two homogeneous media can be expressed as [6], [7]:

$$\begin{bmatrix} E_\mathrm{sh} \\ E_\mathrm{sv} \end{bmatrix} = jk\frac{e^{jkr}}{4\pi r} \begin{pmatrix} S_\mathrm{hh} & S_\mathrm{vh} \\ S_\mathrm{hv} & S_\mathrm{vv} \end{pmatrix} \begin{bmatrix} E_\mathrm{0h} \\ E_\mathrm{0v} \end{bmatrix} I_{\mathrm{A}_0}\,, \tag{3}$$

where E_0h and E_0v are the complex amplitudes of the horizontal and vertical components of the incident field, respectively; $\underline{\underline{S}}$ is the scattering matrix and depends upon the transmitting and receiving polarization states, the dielectric properties of the media, the incident $\hat{k}_\mathrm{i}$ and scattered $\hat{k}_\mathrm{s}$ propagation directions and the unit vector normal to the surface A_0 [6]. It is worth noting that, in presence of a random rough surface, for the evaluation of the scattering matrix the unit vector normal to the surface is evaluated according to the specular reflection law under GO, whereas it is approximated with the unit vector normal to the surface mean plane under zero-order PO [6]. Finally, the scattering integral I_{A_0} can be expressed as follows [7]

$$I_{\mathrm{A}_0} = \iint_{\mathrm{A}_0} e^{jk(\eta_x x + \eta_y y + \eta_z z(x,y))}\, dxdy \tag{4}$$

where $\underline{\eta} = \hat{k}_\mathrm{i} - \hat{k}_\mathrm{s}$ is the wavevector difference, $\hat{k}_\mathrm{s} = \sin\theta_\mathrm{s}\cos\phi_\mathrm{s}\hat{x} + \sin\theta_\mathrm{s}\sin\phi_\mathrm{s}\hat{y} + \cos\theta_\mathrm{s}\hat{z}$ is the scattering direction and I_{A_0} accounts for the statistical description of the surface height $z(x, y)$. Again, if A_0 denotes a random surface, the scattering integral and, then, the scattered EM field are random themselves and cannot be expressed in analytical form. Conversely, closed-form expressions for the mean value $\langle I_{\mathrm{A}_0}\rangle$ and the variance $\sigma^2_{\mathrm{A}_0}$ of $\underline{E}_\mathrm{s}$ can be derived. To this end, different strategies are adopted for the evaluation of the scattering integral under GO and PO, as known in classical theory of EM scattering [4], [5].

Some comments are in order. According to (3), the scattered EM field relevant to the single- and multiple-bounce terms is completely characterized by the scattering matrix and the scattering integral, whose expressions are reported here for the scattering problem shown in Fig. 1. Triple-bounce scattering is here neglected due to its weaker impact on the overall scattered field with respect to lower-order reflections [6], [7], [9]. Additionally, the single-scattering term from the building roof is deterministic due to the smoothness of building faces. It is not reported here for the sake of brevity and can be found in [7]. Finally, the scattering matrix exhibits peculiar symmetries under KA as highlighted in [10]. In particular, it has been demonstrated that S_vv can be derived from S_hh (and vice versa) and S_hv from S_vh (and vice versa), see [10, eq. (35)] and [10, Appendix A] for single and multiple bounces, respectively. Accordingly, here we report closed-form expressions for S_hh, S_vh (first row of the scattering matrix, see (3)), the mean value and variance of the scattering integral relevant to single-bounce from the rough ground (see

TABLE I
SINGLE-SCATTERING FROM GROUND

$$S_\mathrm{hh} = \sin\phi_\mathrm{s}\left[R^\mathrm{G}_\perp(\theta)(\cos\theta + \cos\theta_\mathrm{s}) + (\cos\theta_\mathrm{s} - \cos\theta)\right]$$

$$S_\mathrm{vh} = \cos\phi_\mathrm{s}\left[R^\mathrm{G}_{/\!/}(\theta)(1 + \cos\theta\cos\theta_\mathrm{s}) + (1 - \cos\theta\cos\theta_\mathrm{s})\right]$$

$$\langle I_{\mathrm{A_G}}\rangle = \mathrm{A_G}\ \exp\left(-\frac{k^2\sigma^2\eta_z^2}{2}\right)\mathrm{sinc}\left(\frac{ka\eta_y}{2}\right)\mathrm{sinc}\left(\frac{kb\eta_x}{2}\right)$$

$$\begin{aligned} \mathrm{A_G} &= ab \\ \eta_x &= -\sin\theta_\mathrm{s}\cos\phi_\mathrm{s} \\ \eta_y &= -\sin\theta - \sin\theta_\mathrm{s}\sin\phi_\mathrm{s} \\ \eta_z &= -\cos\theta - \cos\theta_\mathrm{s} \end{aligned}$$

Authorized licensed use limited to: Universita degli Studi di Napoli Federico II. Downloaded on January 05,2021 at 14:20:17 UTC from IEEE Xplore. Restrictions apply.

TABLE II
DOUBLE SCATTERING CONTRIBUTION (WALL-GROUND)

$$S_{\mathrm{hh}} = \frac{2\sin\theta\cos\phi_m}{|\sin\psi_1|^2}\Bigg\{ -\sin(2\phi_m+\phi_\mathrm{s})\left[R_\perp^\mathrm{G}(\theta)(\cos\theta+\cos\theta_\mathrm{s})+(\cos\theta_\mathrm{s}-\cos\theta)\right]\left[R_\perp^\mathrm{W}(\psi_1)\cos^2\theta\cos^2\phi_m - R_{/\!/}^\mathrm{W}(\psi_1)\sin^2\phi_m\right]$$
$$-\cos(2\phi_m+\phi_\mathrm{s})\cos\theta\sin\phi_m\cos\phi_m\left[R_{/\!/}^\mathrm{G}(\theta)(1+\cos\theta\cos\theta_\mathrm{s})+(1-\cos\theta_\mathrm{s}\cos\theta)\right]\left[R_\perp^\mathrm{W}(\psi_1)+R_{/\!/}^\mathrm{W}(\psi_1)\right]\Bigg\}$$

$$S_{\mathrm{vh}} = \frac{2\sin\theta\cos\phi_m}{|\sin\psi_1|^2}\Bigg\{ +\sin(2\phi_m+\phi_\mathrm{s})\cos\theta\sin\phi_m\cos\phi_m\left[R_\perp^\mathrm{G}(\theta)(\cos\theta+\cos\theta_\mathrm{s})+(\cos\theta_\mathrm{s}-\cos\theta)\right]\left[R_\perp^\mathrm{W}(\psi_1)+R_{/\!/}^\mathrm{W}(\psi_1)\right]$$
$$-\cos(2\phi_m+\phi_\mathrm{s})\left[R_{/\!/}^\mathrm{G}(\theta)(1+\cos\theta\cos\theta_\mathrm{s})+(1-\cos\theta_\mathrm{s}\cos\theta)\right]\left[R_{/\!/}^\mathrm{W}(\psi_1)\cos^2\theta\cos^2\phi_m - R_\perp^\mathrm{W}(\psi_1)\sin^2\phi_m\right]\Bigg\}$$

$$\psi_1 = \arccos(\sin\theta\cos\phi_m)$$

$$\begin{aligned}\langle I_{\mathrm{A_{WG}}}\rangle =& \mathrm{A_{WG}}\,\mathrm{sinc}\left[\frac{kl_m}{2}\left(\sin\theta\sin\phi_m-\sin\theta_\mathrm{s}\cos(\phi_\mathrm{s}+\phi_m)\right)\right]\mathrm{sinc}\left[\frac{kh\tan\theta}{2}\left(\sin\theta-\sin\theta_\mathrm{s}\sin(\phi_\mathrm{s}+2\phi_m)\right)\right]\\ &\times\exp\left[-\frac{k^2\sigma^2}{2}(\cos\theta+\cos\theta_\mathrm{s})^2\right]\exp\left[\frac{jkh\tan\theta}{2}\left(\sin\theta-\sin\theta_\mathrm{s}\sin(\phi_\mathrm{s}+2\phi_m)\right)\right]\\ &\times\exp\Big\{jk\Big[x_0\left(\sin\theta\sin2\phi_m-\sin\theta_\mathrm{s}\cos\phi_\mathrm{s}\right)+y_0\left(\sin\theta\cos2\phi_m-\sin\theta_\mathrm{s}\sin\phi_\mathrm{s}\right)\Big]\Big\}\end{aligned}$$

$$\mathrm{A_{WG}} = \begin{cases} l_m h\tan\theta\cos\phi_m, & \text{if } \sin(\phi_\mathrm{s}+\phi_m)>0\\ l_m h\left[\tan\theta\cos\phi_m+\tan\theta_\mathrm{s}\sin(\phi_\mathrm{s}+\phi_m)\right], & \text{if } \sin(\phi_\mathrm{s}+\phi_m)\le 0 \text{ and } \theta\ge\tan^{-1}\left(\dfrac{\tan\theta_\mathrm{s}|\sin(\phi_\mathrm{s}+\phi_m)|}{\cos\phi_m}\right)\\ 0, & \text{otherwise}\end{cases}$$

$$\begin{aligned}\eta_x &= \sin\theta\sin\phi_m-\sin\theta_\mathrm{s}\cos(\phi_\mathrm{s}+\phi_m)\\ \eta_y &= \sin\theta\cos\phi_m-\sin\theta_\mathrm{s}\sin(\phi_\mathrm{s}+\phi_m)\\ \eta_z &= -\cos\theta-\cos\theta_\mathrm{s}\end{aligned}$$

Table I), and double-bounce scattering from wall to ground (see Table II) and ground to wall (see Table III).

For any scattering term, the variance of the scattering integral can be expressed in terms of the surface A_0 and the wavevector difference $\underline{\eta}$ as follows:

$$\sigma^2_{\mathrm{A}_0} = \langle|I_{\mathrm{A}_0}|^2\rangle - |\langle I_{\mathrm{A}_0}\rangle|^2 = \exp\left(-k^2\sigma^2\eta_z^2\right)\mathrm{A}_0\pi l_\mathrm{c}^2 \cdot\sum_{n=1}^{+\infty}\frac{(k\sigma\eta_z)^{2n}}{n!n}\exp\left[-\frac{k^2l_\mathrm{c}^2}{4n}\left(\eta_x^2+\eta_y^2\right)\right] \quad (5)$$

where $\underline{\eta} = \eta_x\hat{x}+\eta_y\hat{y}+\eta_z\hat{z}$. The surface area and the wavevector difference vary among the different contributions and their expressions are reported in the corresponding tables.

Through Tables I-III, a and b stand for the dimensions of the scattering portion of ground, whereas building horizontal and vertical sizes are denoted with l_m ($m=0,1,2,3$) and h, respectively; $R_\perp$ and $R_{/\!/}$ are the (local) Fresnel reflection coefficients for locally perpendicular and parallel polarizations, respectively. The superscripts G and W refer to ground and wall surfaces, respectively. Finally, the local incidence angles are reported as well.

Once the scattered field statistics are computed, the overall RCS of the building can be evaluated as

$$\mathrm{RCS} = 4\pi r^2\frac{\langle|\underline{E}_\mathrm{s}(\underline{r})|^2\rangle}{|E_0|^2} \quad (6)$$

according to the procedure illustrated in [6] for the combination of coherent and incoherent components.

III. SIMULATION RESULTS

By following the rationale and expressions reported in Section II, here we show some simulation results of the proposed bistatic scattering model of the canonical building. Simulation parameters are listed in Table IV.

Figure 2 shows the RCS of the composite target in the θ_s-ϕ_s plane for horizontal-transmit horizontal-receive (HH) polarization and for building orientation angle ranging from 0° to 180° with angular steps of 30°. As it is physically expected, largest RCS is in the specular reflection direction (i.e., for $\theta_\mathrm{s}=\theta$ and $\phi_\mathrm{s}=270^\circ$), where the single-scattering contribution from the smooth building roof is dominant. However, due to the corner-like structure formed by the building walls and the surrounding ground, a strong return is measured in the backscattering region, i.e., for $\phi_\mathrm{s}\in[0^\circ,180^\circ]$. There, the double-bounce scattering terms dominates over the return from the roof and are responsible for the brilliant appearance

Authorized licensed use limited to: Universita degli Studi di Napoli Federico II. Downloaded on January 05,2021 at 14:20:17 UTC from IEEE Xplore. Restrictions apply.

TABLE III
DOUBLE SCATTERING CONTRIBUTION (GROUND-WALL)

$$
\begin{aligned}
S_{\mathrm{hh}} =& \frac{2\sin\theta_{\mathrm{s}}\sin(\phi_m+\phi_{\mathrm{s}})}{|\sin\psi_2|^2}\times \\
&\Big\{-\sin(2\phi_m+\phi_{\mathrm{s}})\left[R_{\perp}^{\mathrm{G}}(\theta)(\cos\theta+\cos\theta_{\mathrm{s}})+(\cos\theta_{\mathrm{s}}-\cos\theta)\right]\left[R_{\perp}^{\mathrm{W}}(\psi_2)\cos^2\theta_{\mathrm{s}}\sin^2(\phi_m+\phi_{\mathrm{s}})-R_{/\!/}^{\mathrm{W}}(\psi_2)\cos^2(\phi_m+\phi_{\mathrm{s}})\right] \\
&-\cos(2\phi_m+\phi_{\mathrm{s}})\cos\theta_{\mathrm{s}}\sin(\phi_m+\phi_{\mathrm{s}})\cos(\phi_m+\phi_{\mathrm{s}})\left[R_{\perp}^{\mathrm{G}}(\theta)(1+\cos\theta\cos\theta_{\mathrm{s}})+(1-\cos\theta_{\mathrm{s}}\cos\theta)\right]\left[R_{\perp}^{\mathrm{W}}(\psi_2)+R_{/\!/}^{\mathrm{W}}(\psi_2)\right]\Big\}
\end{aligned}
$$

$$
\begin{aligned}
S_{\mathrm{vh}} =& \frac{2\sin\theta\sin(\phi_m+\phi_{\mathrm{s}})}{|\sin\psi_2|^2}\times \\
&\Big\{+\cos(2\phi_m+\phi_{\mathrm{s}})\left[R_{/\!/}^{\mathrm{G}}(\theta)(1+\cos\theta\cos\theta_{\mathrm{s}})+(1-\cos\theta_{\mathrm{s}}\cos\theta)\right]\left[R_{\perp}^{\mathrm{W}}(\psi_2)\cos^2\theta_{\mathrm{s}}\sin^2(\phi_m+\phi_{\mathrm{s}})-R_{/\!/}^{\mathrm{W}}(\psi_2)\cos^2(\phi_m+\phi_{\mathrm{s}})\right] \\
&-\sin(2\phi_m+\phi_{\mathrm{s}})\cos\theta_{\mathrm{s}}\sin(\phi_m+\phi_{\mathrm{s}})\left[R_{/\!/}^{\mathrm{G}}(\theta)(\cos\theta+\cos\theta_{\mathrm{s}})+(\cos\theta_{\mathrm{s}}-\cos\theta)\right]\left[R_{\perp}^{\mathrm{W}}(\psi_2)+R_{/\!/}^{\mathrm{W}}(\psi_2)\right]\Big\}
\end{aligned}
$$

$$\psi_2 = \arccos[\sin\theta_{\mathrm{s}}\sin(\phi_m+\phi_{\mathrm{s}})]$$

$$
\begin{aligned}
\langle I_{\mathrm{A_{GW}}}\rangle_{\mathrm{ill}} =& \mathrm{A_{GW}}\,\mathrm{sinc}\left[\frac{kl_m}{2}\left(\sin\theta\sin\phi_m-\sin\theta_{\mathrm{s}}\cos(\phi_{\mathrm{s}}+\phi_m)\right)\right]\mathrm{sinc}\left[\frac{kh\tan\theta_{\mathrm{s}}}{2}\left(\sin\theta\sin\phi_{\mathrm{s}}+\sin\theta_{\mathrm{s}}\cos(\phi_{\mathrm{s}}+2\phi_m)\right)\right] \\
&\times\exp\left[-\frac{k^2\sigma^2}{2}\left(\cos\theta+\cos\theta_{\mathrm{s}}\right)^2\right]\exp\left[\frac{-jkh\tan\theta_{\mathrm{s}}}{2}\left(\sin\theta\sin\phi_{\mathrm{s}}+\sin\theta_{\mathrm{s}}\cos(\phi_{\mathrm{s}}+2\phi_m)\right)\right] \\
&\times\exp\left\{-jk\left[x_0\sin\theta_{\mathrm{s}}\cos\left(\phi_{\mathrm{s}}+2\phi_m\right)+y_0\left(\sin\theta-\sin\theta_{\mathrm{s}}\sin\left(\phi_{\mathrm{s}}+2\phi_m\right)\right)\right]\right\}
\end{aligned}
$$

$$\langle I_{\mathrm{A_{GW}}}\rangle_{\mathrm{sh}} = \langle I_{\mathrm{A_{GW}}}\rangle_{\mathrm{ill}}\exp\left[-jkl_m\left(\sin\theta\cos\phi_m+\sin\theta_{\mathrm{s}}\sin(\phi_{\mathrm{s}}+\phi_m)\right)\right]$$

$$
\mathrm{A_{GW}} = \begin{cases} l_m h\tan\theta_{\mathrm{s}}\sin\left(\phi_{\mathrm{s}}+\phi_m\right), & \text{if } \cos\phi_m>0 \text{ and } \sin\left(\phi_{\mathrm{s}}+\phi_m\right)>0 \\ l_m h[\tan\theta_{\mathrm{s}}\sin\left(\phi_{\mathrm{s}}+\phi_m\right)+\tan\theta\cos\phi_m], & \text{if } \cos\phi_m<0 \text{ and } \sin\left(\phi_{\mathrm{s}}+\phi_m\right)>0 \text{ and } \theta\le\tan^{-1}\left(\dfrac{\tan\theta_{\mathrm{s}}\sin\left(\phi_{\mathrm{s}}+\phi_m\right)}{\cos\phi_m}\right) \\ 0, & \text{otherwise} \end{cases}
$$

$$
\begin{aligned}
\eta_x &= +\sin\theta\sin\phi_m-\sin\theta_{\mathrm{s}}\cos(\phi_{\mathrm{s}}+\phi_m) \\
\eta_y &= -\sin\theta\cos\phi_m+\sin\theta_{\mathrm{s}}\sin(\phi_{\mathrm{s}}+\phi_m) \\
\eta_z &= -\cos\theta-\cos\theta_{\mathrm{s}}
\end{aligned}
$$

of buildings in monostatic SAR imagery [2]. However, in the backscattering region, the direction of the RCS maximum shifts with the building orientation and coincides with the backscattering direction (where $\theta_{\mathrm{s}}=\theta$ and $\phi_{\mathrm{s}}=90^\circ$) only for ϕ multiple of 90°, i.e., for building facing the transmitting antenna. Finally, it is worth mentioning that, as opposed to large-roughness regime where scattering from ground can be properly described using GO as in [7] and [8], largest RCS values in the backscattering direction are due to the coherent scattering component instead of the incoherent one (i.e., EM field variance). Additionally, the incoherent component dominates over the coherent one for very large scattering look angles. However, neither GO nor PO approximations hold for such large angles, due to the shadowing effects neglected in KA.

IV. CONCLUSIONS

In this paper we have presented an analytical model for the evaluation of the EM scattering from a canonical urban scene in bistatic configuration. The composite target analyzed here comprises an isolated building, modeled as a rectangular parallelepiped with smooth dielectric faces, placed on a rough terrain whose roughness has been modeled as a normally-distributed stochastic process. The scattering model has been derived under the framework of KA, with subsequent GO and zero-order PO approximations adopted for describing the EM behavior of building faces and ground, respectively. Indeed,

TABLE IV
SIMULATION PARAMETERS

Parameter	Value
Frequency	1.5GHz
Polarization	HH
Incidence angle	30°
Building orientation	varying
Building size	$20\times20\times30$ m^3
Building relative permittivity	$4-j0.1$
Ground surface height std. dev.	0.003 m
Ground surface correlation length	0.05 m
Ground relative permittivity	$4-j0.1$

Authorized licensed use limited to: Universita degli Studi di Napoli Federico II. Downloaded on January 05,2021 at 14:20:17 UTC from IEEE Xplore. Restrictions apply.

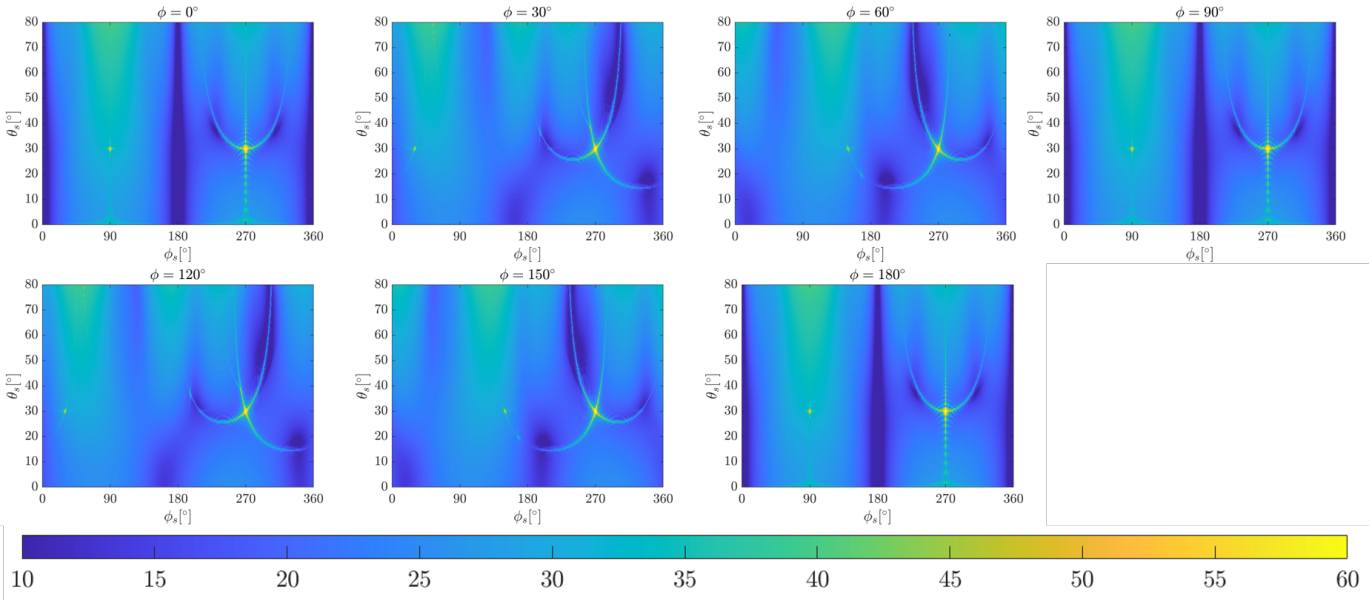

Fig. 2. RCS in dBsm of the canonical building in the θ_s-ϕ_s plane for HH polarization and assuming building orientation ϕ from 0° to 180° with step of 30°. Remaining parameters are set according to Table IV.

in realistic urban scenarios it is expected that PO solution exhibits higher accuracy with respect to GO in modeling the microwave EM return from typical urban ground surfaces, which are characterized by low roughness regimes.

Numerical results show the impact of the building orientation on the overall RCS and highlight the non-negligible effect of the double-bounce mechanism arising from the EM interaction between the building walls and the surrounding ground.

The proposed scattering model can be exploited in inversion algorithms for the retrieval of both geometrical and electromagnetic properties of buildings using bistatic radar data.

Future research lines may regard the derivation of analytical models under surface anisotropy as in [8] and also possibly including multiple adjacent buildings with arbitrary distances, orientation and material composition. Additionally, a comprehensive validation of the proposed model using real bistatic datasets acquired at different orientation angles is also desirable.

Finally, it is worth mentioning that the considered scattering problem might be of interest in ocean environments as well, where maritime surveillance applications, e.g., ship detection/tracking, using space-based bistatic radars, e.g., Global Navigation Satellite Radars-Reflectometry, are experiencing a growing interest in the scientific community as demonstrated by recent works [11]–[16].

REFERENCES

[1] C. Marin, F. Bovolo, and L. Bruzzone, "Building change detection in multitemporal very high resolution SAR images," *IEEE Transactions on Geoscience and Remote Sensing*, vol. 53, no. 5, pp. 2664–2682, 2015.

[2] R. Guida, A. Iodice, and D. Riccio, "Height retrieval of isolated buildings from single high-resolution SAR images," *IEEE Transactions on Geoscience and Remote Sensing*, vol. 48, no. 7, pp. 2967–2979, 2010.

[3] R. Guida, A. Iodice, D. Riccio, and U. Stilla, "Model-based interpretation of high-resolution SAR images of buildings," *IEEE Journal of Selected Topics in Applied Earth Observations and Remote Sensing*, vol. 1, no. 2, pp. 107–119, 2008.

[4] F. T. Ulaby, R. K. Moore, and A. K. Fung, *Microwave Remote Sensing*. Reading, MA, USA: Artech House, 1982, vol. II.

[5] L. Tsang and J. A. Kong, *Scattering of Electromagnetic Waves: Advanced Topics*. New York, NY, USA: John Wiley and Sons, 2001.

[6] G. Franceschetti, A. Iodice, and D. Riccio, "A canonical problem in electromagnetic backscattering from buildings," *IEEE Transactions on Geoscience and Remote Sensing*, vol. 40, no. 8, pp. 1787–1801, 2002.

[7] A. Di Simone, W. Fuscaldo, L. M. Millefiori, D. Riccio, G. Ruello, P. Braca, and P. Willett, "Analytical models for the electromagnetic scattering from isolated targets in bistatic configuration: Geometrical Optics solution," *IEEE Transactions on Geoscience and Remote Sensing*, vol. 58, no. 2, pp. 861–880, Feb. 2020.

[8] G. Di Martino, A. Di Simone, W. Fuscaldo, A. Iodice, D. Riccio, and G. Ruello, "Electromagnetic scattering from a canonical target over an anisotropic rough surface using Geometrical Optics," in *2020 XXXIIIrd General Assembly and Scientific Symposium of the International Union of Radio Science (URSI GASS)*, 2020.

[9] A. Di Simone and *et al.*, "Analytical models for the electromagnetic scattering from isolated targets in bistatic configuration: Zero-order Physical Optics solution," *IEEE Transactions on Geoscience and Remote Sensing*, unpublished.

[10] W. Fuscaldo, A. Di Simone, L. M. Millefiori, A. Iodice, P. Braca, and P. Willett, "A convenient analytical framework for electromagnetic scattering from composite targets," *Radio Science*, vol. 54, no. 8, pp. 785–807, 2019.

[11] A. Di Simone, H. Park, D. Riccio, and A. Camps, "Sea target detection using spaceborne GNSS-R delay-Doppler maps: Theory and experimental proof of concept using TDS-1 data," *IEEE Journal of Selected Topics in Applied Earth Observations and Remote Sensing*, vol. 10, no. 9, pp. 4237–4255, 2017.

[12] A. Di Simone, A. Iodice, D. Riccio, A. Camps, and H. Park, "GNSS-R: A useful tool for sea target detection in near real-time," in *2017 IEEE 3rd International Forum on Research and Technologies for Society and Industry (RTSI)*. Modena, Italy: IEEE, 2017, pp. 1–6.

[13] T. Beltramonte, P. Braca, M. Di Bisceglie, A. Di Simone, C. Galdi, A. Iodice, L. M. Millefiori, D. Riccio, and P. Willett, "Simulation-based feasibility analysis of ship detection using GNSS-R delay-Doppler maps," *Journal of Selected Topics in Applied Earth Observations and Remote Sensing*, vol. 13, pp. 1385–1399, 2020.

Authorized licensed use limited to: Universita degli Studi di Napoli Federico II. Downloaded on January 05,2021 at 14:20:17 UTC from IEEE Xplore. Restrictions apply.

[14] M. P. Clarizia, P. Braca, C. S. Ruf, and P. Willett, "Target detection using GPS signals of opportunity," in *2015 18th International Conference on Information Fusion (FUSION)*, Washington, DC, USA, July 6–9, 2015, pp. 1429–1436.

[15] B. J. Southwell, J. W. Cheong, and A. G. Dempster, "A matched filter for spaceborne GNSS-R based sea-target detection," *IEEE Transactions on Geoscience and Remote Sensing*, pp. 1–10, 2020.

[16] J. W. Cheong, B. J. Southwell, and A. G. Dempster, "Blind sea clutter suppression for spaceborne GNSS-R target detection," *IEEE Journal of Selected Topics in Applied Earth Observations and Remote Sensing*, vol. 12, no. 12, pp. 5373–5378, 2019.

Authorized licensed use limited to: Universita degli Studi di Napoli Federico II. Downloaded on January 05,2021 at 14:20:17 UTC from IEEE Xplore. Restrictions apply.